THE BENCHMARK CALCULATIONS OF THE GAMMA+ CODE WITH THE HTR-10 SAFETY DEMONSTRATION EXPERIMENTS

JI SU JUN*, HONG SIK LIM and WON JAE LEE
Korea Atomic Energy Research Institute
P.O.Box105, Yuseong, Daejeon, Korea 305-600
*Corresponding author. E-mail : junjisu@kaeri.re.kr

Received June 23, 2008
Accepted for Publication October 20, 2008

KAERI (Korea Atomic Energy Research Institute) has developed the GAMMA+ code for a thermo-fluid and safety analysis of a VHTR (Very High Temperature Gas-Cooled Reactor). A key safety issue of the VHTR design is to demonstrate its inherent safety features for an automatic reactor power trip and power stabilization during an anticipated transient without scram (ATWS) accident such as a loss of forced cooling by a trip of the helium circulator (LOFC) or a reactivity insertion by a control rod withdrawal (CRW). This paper intends to show the ATWS assessment capability of the GAMMA+ code which can simulate the reactor power response by solving the point-kinetic equations with six-group delayed neutrons, by considering the reactivity changes due to the effects of a core temperature variation, xenon transients, and reactivity insertions. The present benchmark calculations are performed by using the safety demonstration experiments of the 10 MW high temperature gas-cooled-test module (HTR-10) in China. The calculation results of the power response transients and the solid core temperature behavior are compared with the experimental data of a LOFC ATWS test and two CRW ATWS tests by using a 1mk-control rod and a 5mk-control rod, respectively. The GAMMA+ code predicts the power response transients very well for the LOFC and CRW ATWS tests in HTR-10.

KEYWORDS : LOFC, CRW, ATWS Accidents, Reactivity Feedback, HTR-10, Power Response

1. INTRODUCTION

KAERI has established a plan for an ecological environment and an economical energy supply to demonstrate a massive production of hydrogen using a VHTR by the early 2020s [1]. The GAMMA (GAs Multicomponent Mixture Analysis) [2] code has been developed for the thermo-fluid and safety analysis tool of the VHTR design. The GAMMA+ code can predict the thermo-fluid and chemical reaction behavior during an air ingress accident as well as simulate the reactor power transient response by solving the point-kinetic equations [3] with six-group delayed neutrons, by considering the reactivity changes due to the effects of a core temperature variation, xenon transients and intentional reactivity insertions such as control rod withdrawal.

An anticipated transient such as the loss of the helium flow circulator without a reactor scram or a control rod withdrawal without a reactor scram are key safety demonstration issues of the VHTR design. That is, the VHTR design is required to show its inherent safety features for an automatic reactor power decrease and a power stabilization due to the negative reactivity feedback caused by a temperature rise in the core after ATWS accidents, even when the shut down control rod is not inserted. This study intends to show the capability of the GAMMA+ code to predict ATWS accidents.

The present benchmark calculations use the HTR-10 experiments of the LOFC ATWS and the CRW ATWS. The test data [4,5] are provided by a joint project between KAERI and INET (the Institute of Nuclear Energy Technology) in China. The HTR-10 reactor [6] is a pebble-bed type, graphite-moderated and high temperature helium gas-cooled test module with a thermal power of 10 MW and a reactor outlet temperature of 700 °C. The GAMMA+ code has already demonstrated a good prediction capability for a steady state temperature distribution of the HTR-10 Full Power Initial Core (FPIC) with less than a ±10% deviation [7,8]. HTR-10 ATWS tests were performed at 30% rated power conditions with an outlet helium temperature of 650 °C. Using the fluid part, solid part and boundary models of the HTR-10 system for the FPIC benchmark calculation, the ATWS calculations are applied for a LOFC test [9] and two CRW tests [10] by using a

1mk-control rod and a 5mk-control rod, respectively. The main results of the power response transients during the ATWS accidents are compared with the experimental data. The calculation results provide the net reactivity behavior including the reactivity feedback effects of the fuel temperature, moderator temperature, reflector temperature, xenon concentration, and a control rod. The transient behaviors of the solid temperatures in the core, the outlet helium temperature and the maximum fuel temperature are also examined.

For the applications of the coupled neutronics/thermal-hydraulics codes for the PBMR (Pebble-Bed Modular Reactor), MARS-GCR/CAPP codes [11] have been used for the coupled multi-physics/thermal-hydraulics transient calculation of the PBMR-400 core design. As the code-to-code benchmark, the calculation results were compared with those of other coupled neutronics/thermal-hydraulics codes such as PARCS/THERMIX, TINTE, DORT/THERMIX and DALTON/THERMIX. As the code-to-experimental benchmark, the participants at the IAEA CRP-5 RCM-7 meeting have presented their calculation results for the same HTR-10 benchmark problems [12] using coupled neutronics/thermal-hydraulics codes such as THERMIX-KONVEK-KINEX, TAC-NC, PANTHERMIX, TINTE and GRSAC. But, this paper is not concerned with their results because the final results have not been published.

2. CALCULATION METHOD

2.1 GAMMA+ Code Models

The GAMMA code [2] was developed to predict thermo-fluid transients including the air ingress phenomena in a VHTR. The fluid flow and heat transport in the GAMMA code are solved unsteadily by the thermal non-equilibrium model, consisting of two sets of equations for both the gas and the solid. KAERI has improved the GAMMA code (called GAMMA+) by updating the numerical scheme, by using two solid conduction equations for the fueled zone and the unfueled zone in a composite reactor core made of fuel and graphite, and by implementing point-kinetic equations [3].

As shown in Fig. 1, the solid region in a reactor core is divided into two zones: the fueled zone and the unfueled zone of the graphite matrix. A one-dimensional heat conduction equation is used in the fueled zone without relevance to the fuel's geometric shape, a pebble sphere of PBMR fuel or a compact rod of Prismatic Modular Reactor (PMR) fuel. HTR-10 is a PBMR and uses fuel in the shape of a pebble sphere.

$$\left(\rho C_p\right)_{fuel}\frac{\partial T_{fuel}}{\partial t}=\frac{1}{\xi}\frac{\partial}{\partial r}\left(\xi\lambda_{fuel}\frac{\partial T_{fuel}}{\partial r}\right)+\dot{q}_N'''-\dot{q}_{gf}''' \qquad (1)$$

where $\dot{q}_N'''$ is a volumetric nuclear heat production and $\dot{q}_{gf}'''$ is a heat exchange term between the fueled zone and the unfueled graphite zone. ξ is r for a compact rod or r^2 for a pebble sphere.

In the unfueled zone, a multi-dimensional heat conduction equation is modeled by a continuous porous medium approach [13].

$$\left[(1-\varphi)\varphi_g\left(\rho C_p\right)_w\right]\frac{\partial T_w}{\partial t}=\frac{\partial}{\partial x_i}\left(\lambda_{eff}\frac{\partial T_w}{\partial x_i}\right)-\dot{q}_{sf}'''+\dot{q}_{gf}''' \qquad (2)$$

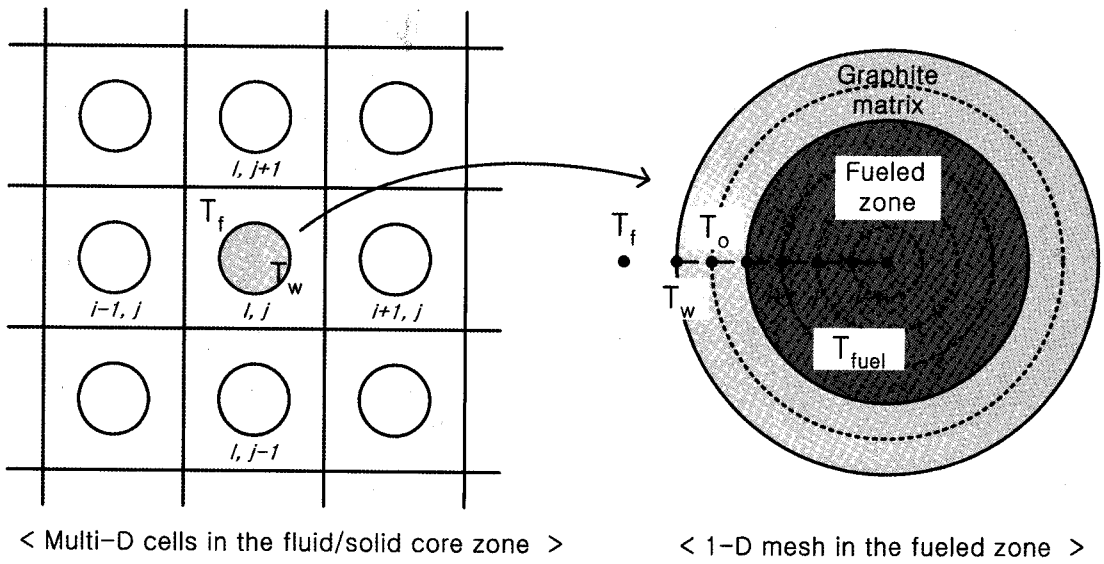

Fig. 1. Two Zone Heat Conduction Models for a Pebble Sphere

where φ is the porosity of the fluid zone and φ_g is the volume fraction of the graphite zone of a fuel and graphite composite. $\dot{q}'''_{sf}$ is a heat exchange term between the fluid and the solid part. λ_{eff} is effective thermal conductivity including the contact conductance, gas conductance and void radiation.

The heat conduction equations are discretized by the Crank-Nicolson method [14] in a time scheme and the finite volume method in a grid scheme.

The discretized 1-D heat conduction of the fueled zone is finally expressed as the following:

$$a_i T_{i-1} + b_i T_i + c_i T_{i+1} = d_i$$

$$a_i = -\frac{\lambda_{fuel}\xi_{i-1}}{r_i - r_{i-1}} \qquad b_i = \frac{(\rho Cp_i)}{\Delta t} - a_i - c_i$$

$$c_i = -\frac{\lambda_{fuel}\xi_i}{r_{i+1} - r_i} \qquad d_i = \frac{(\rho Cp_i)}{\Delta t} T_i + q_{N_i} \tag{3}$$

In the above equation, the fuel temperature (T_o) at the outer mesh of the first inner point from the surface is unknown and expressed as a function of the surface temperature (T_w) of a fuel and graphite composite as the following.

$$T_o = A_I^{-1} d_I - A_I^{-1}(c_I T_w) = B_v - B_s T_w \tag{4}$$

where A^{-1} is the inverse matrix of A, which is the coefficient matrix of the left hand side in equation (3). In the multi-dimensional heat conduction equation (2), the heat transfer between the fueled zone and the unfueled graphite zone is defined as the following.

$$\dot{q}'''_{gf} = h_g a_{gf}\left(T_{o_{i,j}} - T_{w_{i,j}}\right) \tag{5}$$

where h_g is a heat conductance of the graphite and a_{gf} is the specific surface area per volume. By defining $h_{gf} = h_g a_{gf}$ and inserting equation (4) into equation (5), $\dot{q}'''_{gf}$ is expressed as a function of T_w only as the following.

$$\dot{q}'''_{gf} = h_{gf_{i,j}} B_{vi,j} - h_{gf_{i,j}}\left[1 + B_{si,j}\right] T_{w_{i,j}} \tag{6}$$

Then, discretized by the multi-dimensional cells in the core zone as shown in Fig. 1, the heat conduction equation (2) is finally expressed as the following.

$$a_c T_{i,j} + a_w T_{i-1,j} + a_e T_{i+1,j} + a_b T_{i,j-1} + a_t T_{i,j+1} = b_{ij} \tag{7}$$

$$a_w = -\frac{1}{Vol_{ij}}\frac{\left(A_x\lambda_{eff}\right)_{i-1/2,j}}{\Delta x_{i-1/2}} \quad a_e = -\frac{1}{Vol_{ij}}\frac{\left(A_x\lambda_{eff}\right)_{i+1/2,j}}{\Delta x_{i+1/2}} \quad a_b = -\frac{1}{Vol_{ij}}\frac{\left(A_z\lambda_{eff}\right)_{i,j-1/2}}{\Delta z_{j-1/2}}$$

$$a_t = -\frac{1}{Vol_{ij}}\frac{\left(A_z\lambda_{eff}\right)_{i,j+1/2}}{\Delta z_{i+1/2}}$$

$$a_c = (1-\varphi)\varphi_g\left(\rho C_p\right)_{ij}/\Delta t + h_{gf_{i,j}}\left[1 + B_{si,j}\right] - a_w - a_e - a_b - a_t$$

$$b_{ij} = T_{ij}\left[(1-\varphi)\varphi_g\left(\rho C_p\right)_{ij}/\Delta t\right] - q''_{sf\,i,j} + h_{gf_{i,j}} B_{vi,j}$$

Thus, equation (7) is coupled implicitly with the 1-D heat conduction equation (4) by the term $\dot{q}'''_{gf}$ and is coupled explicitly with the fluid governing equations by the term $\dot{q}'''_{sf}$. In this way, the temperature distributions in the unfueled zone and the fueled zone are obtained simultaneously.

In the GAMMA+ code, the reactor power transient is solved by using the point-kinetic equations with six-group delayed neutrons, by considering the reactivity changes caused by the effects of the xenon transients, the core temperature changes, and the intentional reactivity insertions such as a control rod withdrawal. Total thermal power is calculated by a summation of the prompt fission power, the precursor decay power and the delayed fission power.

$$P_{tot} = \left(1 - \sum_{j=1}^{J} E_j\right) P + \sum_{j=1}^{J} \lambda_j^H H_j \tag{8}$$

where P is the prompt fission power, E_j is the effective energy fraction of the decay heat group, λ_j^H is the decay constant of decay heat group and H_j is the power from the decay heat group. Equation (8) is simultaneously coupled with the time-dependent ordinary differential equations of the fission power, the delayed-neutron concentration and the power from the decay heat group. These equations have functions of reactivity, a fraction of the delayed neutrons, a prompt neutron lifetime, and so on. The change of reactivity by xenon concentration is also coupled with the ordinary differential equations of the xenon concentration and the iodine concentration. The ordinary differential equations are solved by the Runge-Kutta Method [14]. Total thermal power of the equation is applied for the volumetric nuclear heat production ($\dot{q}'''_N$) of the equation (1).

2.2 HTR-10 Reactor System

Fig. 2 shows the primary system of the HTR-10 reactor [6], which is a pebble-bed type, graphite-moderated and high temperature helium gas-cooled-test module. The fluid system of the HTR-10 consists of the helium gas cooling system for cooling the reactor core and the Reactor Cavity Cooling System (RCCS) for cooling the air cavity between the Reactor Pressure Vessel (RPV) and the concrete wall. The active core of HTR-10 is cylinder-shaped and cone-shaped at the bottom to unload fuel elements. Graphite

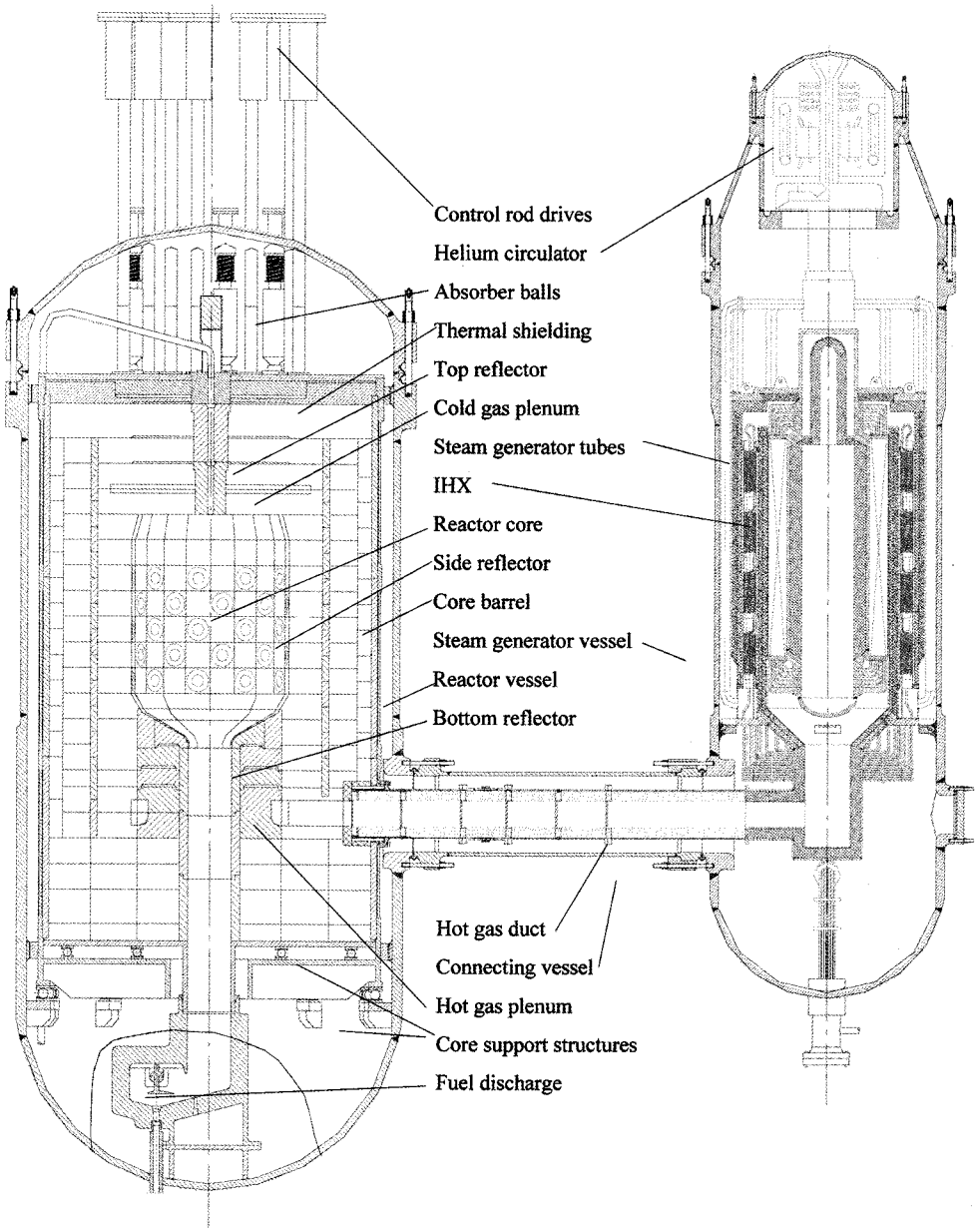

Fig. 2. The HTR-10 Reactor Primary System

reflectors and carbon brick reflectors surround the core at the top, side, and bottom zones. After entering the RPV, the cold helium flows downwards through the annular gap between the core vessel and the RPV. Then the flow changes direction upwardly. A small part of this cold helium is expected to pass directly through the fuel discharging tube to the hot core. The remaining helium goes around the core support structures and a major part of this flow enters the cold helium channels in the side reflector. Table 1 shows the main design parameters of the HTR-10, which has a 10 MW full operating power with a reactor outlet temperature of 700 °C, a reactor inlet temperature of 250 °C, a flow rate of 4.32 kg/s, and a primary helium pressure of 3 MPa.

The GAMMA+ code predicted the steady state temperature distribution in the HTR-10 reactor at FPIC conditions [7,8]. Fig. 3 shows the steady state calculation results of the solid temperature distribution and the prediction error of the GAMMA+ code for the measured solid temperatures at 22 fixed instrumentation positions in HTR-10. This shows overall good predictions with a less than ±10% deviation except for two data points in the fuel discharging tube zones.

The present ATWS benchmark calculations of the

Table 1. Main Design Parameters of the HTR-10

Parameter	Value
Reactor thermal power, MW	10
Primary helium pressure, MPa	3.0
Average helium temperature at reactor outlet, °C	700
Average helium temperature at reactor inlet, °C	250
Helium mass flow rate at full power, kg/s	4.32
Main steam pressure at steam generator outlet, MPa	4.0
Main steam temperature at steam generator outlet, °C	440
Feed water temperature of steam generator, °C	104
Main steam flow rate, kg/s	3.47
Electricity power generated by steam turbine, MW	3.0
Average height of reactor core, m	1.97
Volume of reactor core, m^3	5
Thickness of the top reflector, m	0.9
Thickness of top boronated carbon brick, m	0.4
Equivalent thickness of side reflector graphite, m	0.778
Equivalent thickness of side boronated carbon brick, m	0.222
Number of cold helium flow channels	20
Diameter of cold helium flow channel, m	0.08
Radial coordinate of cold helium flow channel center, m	1.446
Thickness of bottom reflector, m	1.212
Thickness of bottom boronated carbon brick, m	0.3
Thickness of bottom non-boronated carbon brick, m	0.7
Inner diameter of core vessel, m	3.82
Inner diameter of RPV, m	4.2

Table 2. Initial Steady State Conditions for the LOFC and CRW ATWS Tests

Parameter	Value
Reactor power, kW	3315
Inlet helium temperature, °C	212
Outlet helium temperature, °C	650
Primary loop pressure, kPa	2476
Number of fuel balls	13651
Number of graphite dummy balls	16408

HTR-10 reactor used the same code input models for the geometric information, material properties, heat transfers, and RCCS boundary as those used in the FPIC calculation. Fig. 4 shows the helium flow path through the solid core structures. The calculation of the helium cooling system is modeled up to the horizontal co-axial hot gas duct connecting the RPV and the steam generator. The heat generated in the reactor core is cooled by a conduction and radiation heat transfer of the reactor structures as well as by a convective heat transfer of the fluid system. The

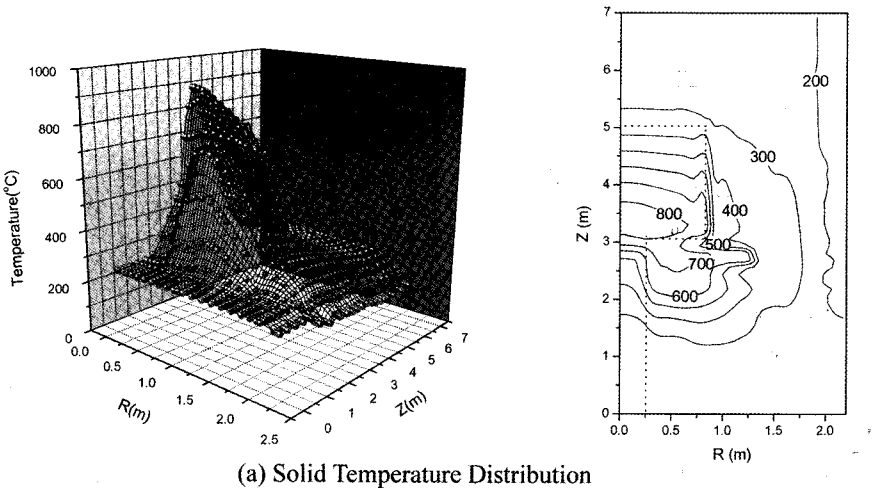

(a) Solid Temperature Distribution

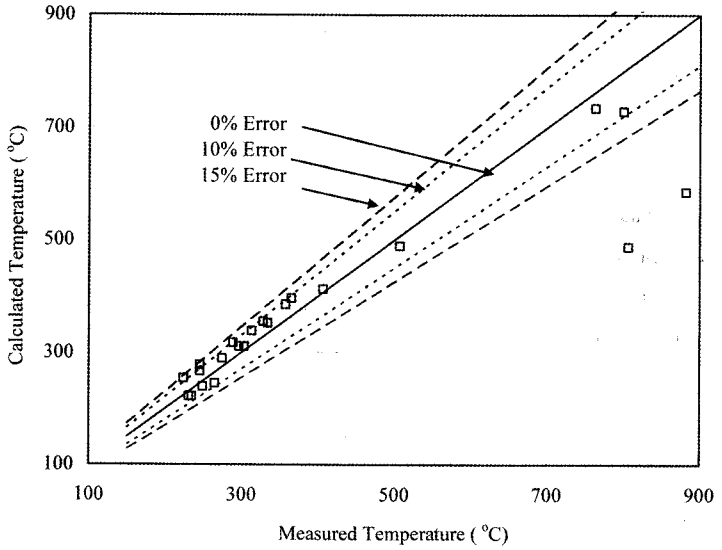

(b) GAMMA+ Code Prediction Error

Fig. 3. Solid Temperature Results at the Steady State FPIC in HTR-10 Reactor

solid part is solved by the 2-D heat conduction equation. The solid parts containing the partial helium zone, such as the control rod channel and the riser channel, are regarded as porous medium. The pebble-bed core has a porosity of 0.39. The radiation in the pebble bed core is considered by the effective thermal conductivity of Zehner-Schluender [13]. This calculation considers the surface radiation heat transfer in the top plenum, helium gap inside the RPV, and the air gap between the RPV and the water cooling tube zones. The radiation heat transfer is modeled by using an irradiation/radiosity method [15], which assumes that the fluid is non-participating and the radiation exchange between the surfaces is gray and diffuse.

2.3 HTR-10 ATWS Tests

The ATWS safety demonstration tests for the HTR-10 reactor were conducted in order to verify the inherent safety features of a VHTR and to obtain the transient data of the power response and the primary cooling system for a validation of the safety analysis code. Table 2 shows the initial steady state operating conditions for both LOFC and CRW ATWS tests in the HTR-10. Xenon equilibrium state was achieved before starting the safety demonstration experiments. There was no heat generation in the lower part of the reactor core and the fuel discharging tube.

The LOFC ATWS test assumes an accident in which the helium circulator is suddenly switched off, but a shut down control rod is not inserted. The CRW test introduces a positive reactivity insertion into the core to simulate an accident of an unexpected control rod withdrawal. Like the LOFC ATWS test, the CRW ATWS test assumes an accident in which the helium circulator trips because of an overpower trip signal after a control rod withdrawal, but a shut down control rod is not inserted into the core in

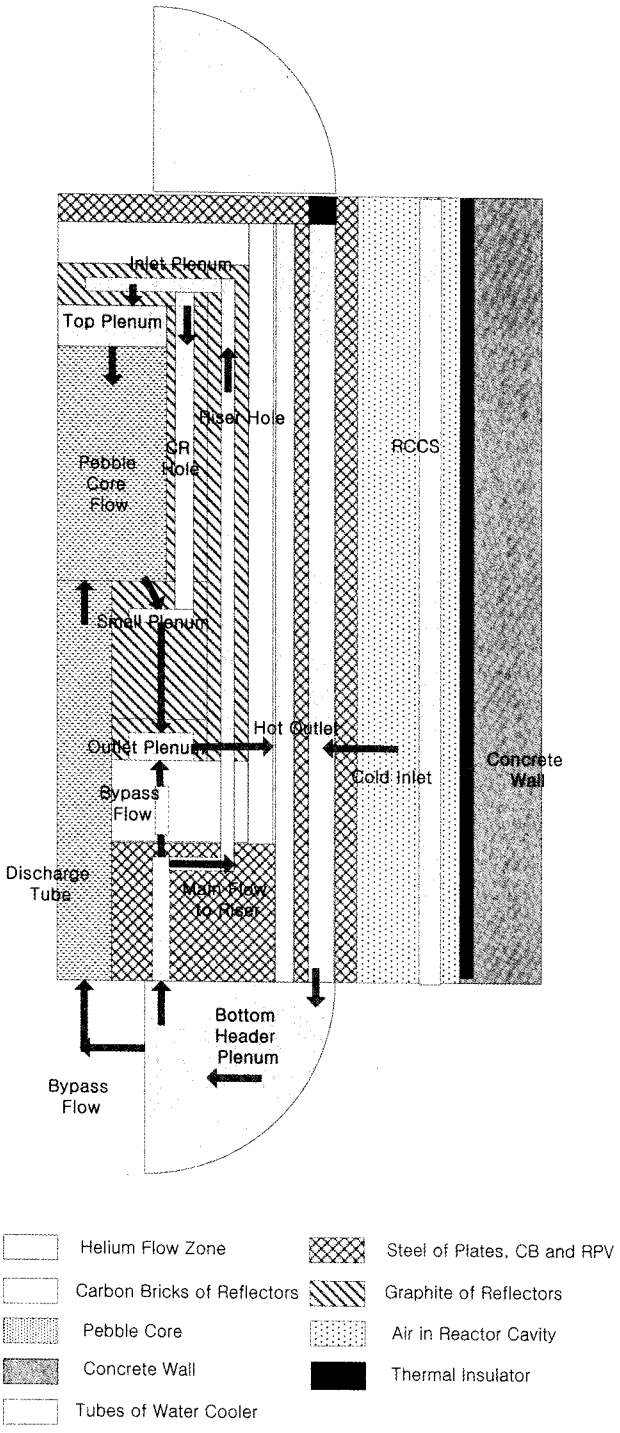

Fig. 4. Helium Flow Path in the HTR-10 Reactor

order to simulate the ATWS. The reactor power increases steadily until the negative reactivity feedback effect in the core is larger than the inserted reactivity. The reactivity insertions were made by two kinds of experiments as shown in Fig. 5. For a small reactivity insertion test, the withdrawal of a 1mk control rod was finished in 20

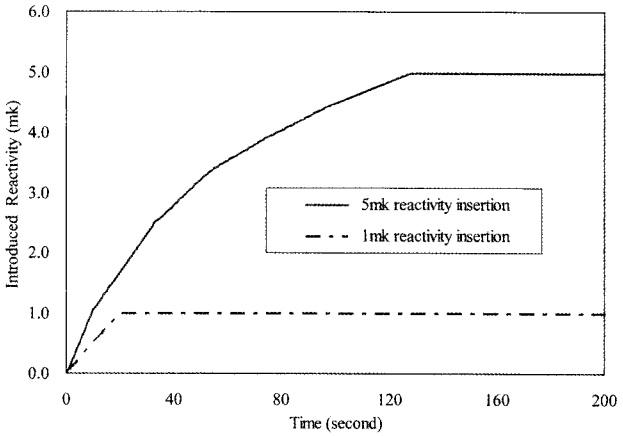

Fig. 5. Reactivity Insertion Variations for the CRW ATWS Tests

seconds. A 4.9762 mk reactivity was slowly inserted by withdrawing a 5mk control rod in 128 seconds for a large reactivity insertion test. The helium circulator trips when the reactor power reaches 3.96 MW at a 120% overpower level when compared to the initial power of 3.3 MW.

The main test objectives are to verify the inherent safety features of an automatic reactor power trip and a power stabilization due to the negative reactivity feedback caused by a rise of the temperature in the core after ATWS tests. These design features are required for the maintenance of the fuel and reactor structure integrity below a temperature limit during ATWS accidents in a VHTR. The main experimental data was the reactor power response behavior after the LOFC or CRW. In addition to the reactor power transient, the test results provided the transient data of some operating parameters such as the inlet/outlet temperatures of the core, the reflector temperature, the pressure of the primary circuit, the temperatures of the pressure vessel and the metal support.

2.4 Calculation Conditions

A flow rate of 1.413 kg/s was used to adjust the initial steady state conditions of Table 2. A temperature of 50 °C at the RCCS water cooling tube [12] was used as a fixed boundary condition through the transients. Table 3 shows the input data [12] for the point-kinetic parameters, which are proven to well simulate the reactor power response after the ATWS due to the reactivity feedback effect.

Simulating the transient power behavior of the ATWS requires not only the point-kinetic parameters but also the time dependent flow conditions such as the flow coastdown, the inlet helium temperature and the outlet helium pressure. The measured data for the inlet temperature and the outlet pressure are directly used for the time dependent boundary conditions because the calculation does not simulate the secondary side. Fortunately, the variations of these parameters are very small during the transients. Based on

Table 3. Point-Kinetic Parameters for the HTR-10

Parameter	Value
Total fraction of delayed neutrons	0.00726
Effective prompt lifetime, seconds	0.00168
Coefficient of fuel temperature, Δk/k/°C	-2.13×10^{-5}
Coefficient of moderator temperature, Δk/k/°C	-16.2×10^{-5}
Coefficient of reflector temperature, Δk/k/°C	7.71×10^{-5}

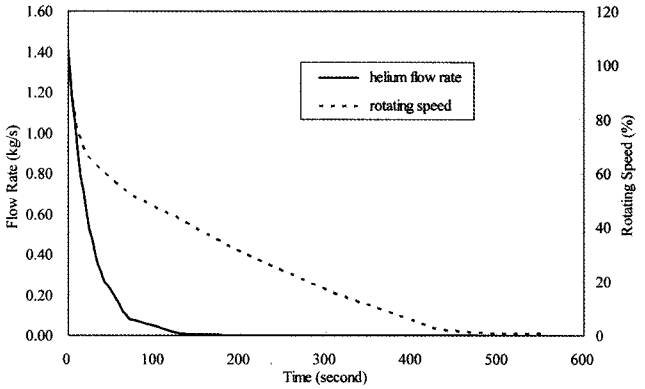

Fig. 6. Flow Coastdown Curve after the Circulator Trip

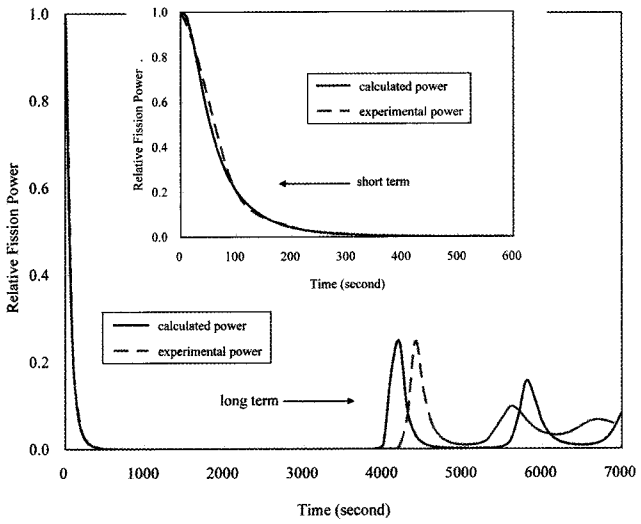

Fig. 7. Reactor Power Transient after the LOFC ATWS

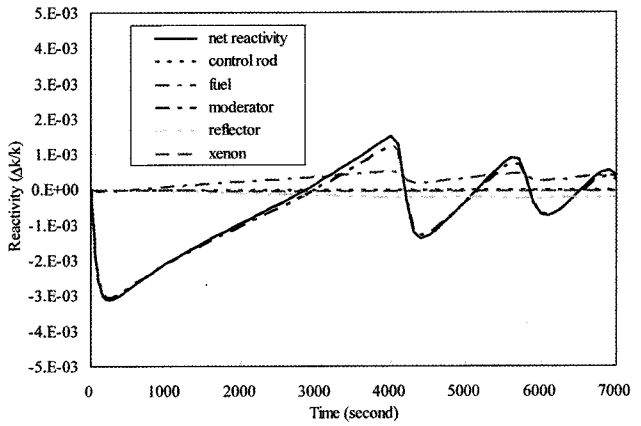

Fig. 8. Reactivity Transient after the LOFC ATWS

the sensitivity study of the various flow coastdown curves, the flow coastdown curve of Fig. 6 is selected by comparing the power decay curve for a short term with the experimental data. The helium flow rate decreases linearly in proportion to the rotation speed in ten seconds and then it rapidly decreases to zero in 150 seconds. This curve is very similar to the ATWS test results [16] of a CRW.

3. CALCULATION RESULTS

3.1 Results of the LOFC ATWS

Fig. 7 compares the calculation results of the power response after the circulator trip with the experimental data. The fission power starts to decrease just after the circulator trip due to the negative reactivity feedback caused by the temperature rise of the pebble core, and reaches zero power in 400 seconds. After the reactor is subcritical for a long time, the core becomes critical again and the power reaches a peak oscillation value at 4200 seconds. The power is oscillated several times by the reactivity feedback due to the change of the core temperature, and is finally stabilized at a low power level. As shown in Fig. 7, the calculated power response is very close to that found in the experimental data of the power decay curve for the short term, and the re-criticality time and the power oscillation peak for the long term. The calculated re-criticality of a 25% power peak at 4200 seconds is very similar to the experimental data of a 25% power peak at 4400 seconds.

Fig. 8 shows the behavior of the net reactivity, including the reactivity feedback effects of the fuel temperature, moderator temperature, reflector temperature, xenon

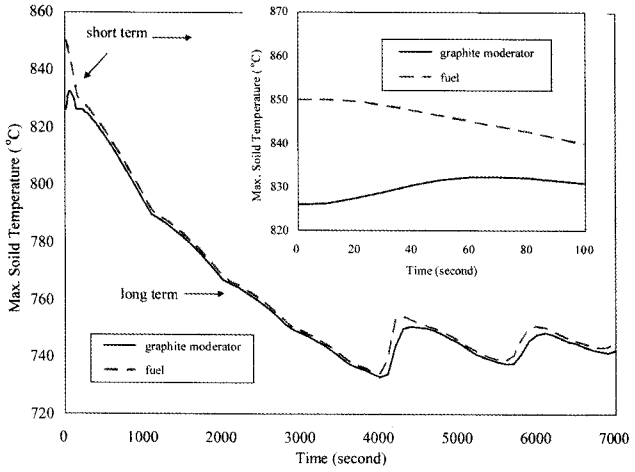

Fig. 9. Maximum Temperature Transient of the Fuel and Graphite Moderator after the LOFC ATWS

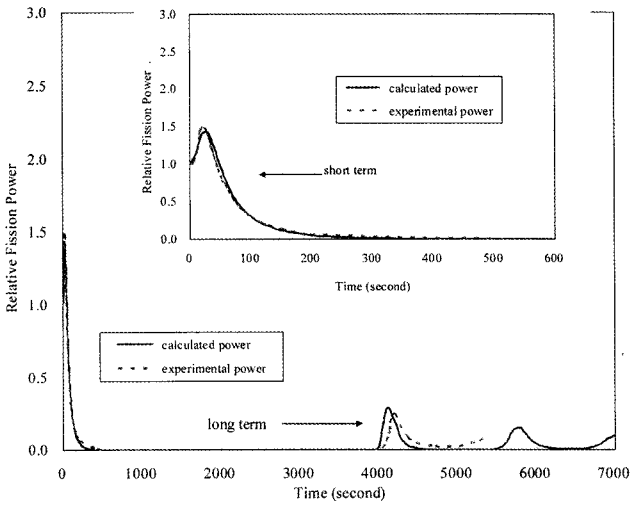

Fig. 10. Reactor Power Transient after the 1mk-CRW ATWS

concentration and control rod. The reactivity of the control rod remains zero because it is not inserted during the LOFC ATWS. The net reactivity decreases rapidly in 240 seconds due to the negative reactivity feedback, and then it increases slowly. The reactor core becomes critical again at 2900 seconds and reaches a re-critical peak reactivity at 4000 seconds. The reactivity of the graphite moderator mainly contributes to the net reactivity behavior, compared to the effects of the fuel, the reflector, and the xenon concentration.

Fig. 9 shows the maximum temperature behaviors of the fuel and the graphite moderator. The maximum fuel temperature is slowly decreased by 116 °C in 4000 seconds (-1.74 °C/min), and then oscillates like the power response. The maximum graphite moderator temperature increases in 70 seconds just after the LOFC due to the instantly large loss of convection heat transfer, and then moderator temperature behaves like the fuel temperature. Although the temperature transients of the fuel and the moderator behave similarly to each other, the graphite moderator mainly contributes to the net reactivity because the coefficient for the moderator temperature is seven times greater than that of the fuel temperature.

3.2 Results of the 1mk CRW ATWS

Fig. 10 compares the calculation results of the power response behavior after withdrawing the 1mk control rod with the experimental data. The reactor power rapidly increases due to the positive reactivity insertion caused by control rod withdrawal. Then, power reaches a 120% overpower in twelve seconds. After the circulator is switched off, the reactor power continuously increases due to the increase of the reactivity insertion and reaches a peak power of 142% overpower in 30 seconds. The calculation result of the reactor power response for the short term is very close to the experimental data, which shows a peak power of a 149% overpower in 22 seconds.

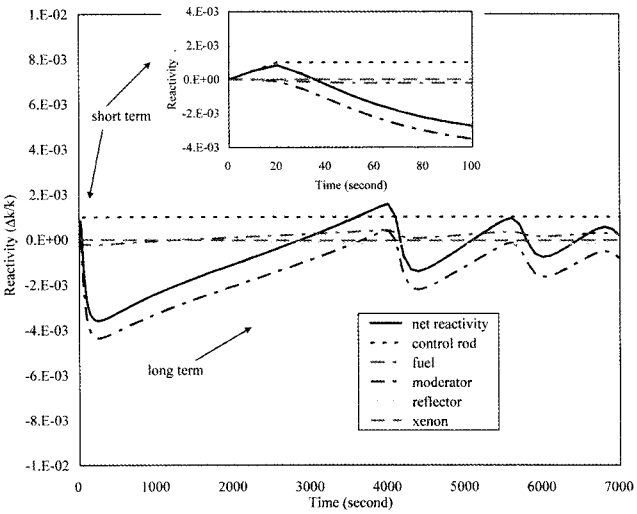

Fig. 11. Reactivity Transient after the 1mk-CRW ATWS

The reactor power starts to decrease due to the negative reactivity feedback corresponding to the rise of the core temperature caused by a power increase and a flow decrease. Then, the fission power rapidly decreases to zero power in 400 seconds, and the reactor is in a subcritical state for a long time. The re-criticality power peak occurs at 4100 seconds with about 28% of the initial power, which is very close to the experimental data of a 25% power peak at 4200 seconds. After that, the power oscillates several times because of the reactivity feedback that stems from the change of the core temperature. The power oscillation peak is decreased and finally stabilized by a stable thermal performance of the graphite structures with a large heat capacity and heat conductivity.

Fig. 11 shows the net reactivity behavior including the reactivity feedback effects of the fuel temperature,

moderator temperature, reflector temperature, xenon concentration, and the control rod after withdrawing the 1mk control rod. The reactivity of the control rod is only an experimental value shown in Fig. 5. The net reactivity reaches a peak at 20 seconds due to the reactivity insertion of the control rod, and then decreases to below zero at 40 seconds when the negative reactivity feedback becomes greater than the inserted reactivity. The net reactivity decreases continuously for 280 seconds due to the negative reactivity feedback, and then slowly increases. The reactor core becomes critical again at 2900 seconds and reaches a re-critical peak reactivity at 4000 seconds. Compared to the small effects of the fuel, the reflector, and xenon density, the reactivities of the graphite moderator and the control rod mainly contribute to the net reactivity behavior.

Fig. 12 shows the maximum temperature behaviors of the fuel and the graphite moderator after withdrawing the 1mk control rod. The maximum fuel temperature increases by about 7 °C in 40 seconds just after withdrawing the control rod due to the power increase, and then slowly decreases by about 115 °C in 4000 seconds (-1.74 °C/min). After that, maximum fuel temperature increases again and oscillates according to the power response. The maximum temperature of the graphite moderator increases by about 12 °C in 80 seconds due to the power increase after the CRW and the instantly large loss of convection heat transfer after the circulator trip, and then the temperature behaves like the fuel temperature. The 1mk reactivity insertion is small, so the behaviors of the reactor power response and the core temperature after the circulator trip are similar to the trends of the LOFC ATWS experiment.

3.3 Results of the 5mk CRW ATWS

Fig. 13 compares the calculation results of the power response behavior after withdrawing the 5mk control rod with the experimental data. Fig. 13 (a) is the result using the flow coastdown curve of Fig. 6, and Fig. 13 (b) shows the result using the slow flow coastdown curve which decreases to zero flow about 50 seconds later than that of Fig. 6.

As shown in Fig. 13 (a), the overall power response behavior is close to the experimental data. Due to a larger reactivity insertion, the reactor power reaches a 120% overpower in seven seconds and a 216% peak power occurs at 30 seconds, which are faster and greater than those of the 1mk reactivity insertion, respectively. The peak power is slightly less than the experimental data of a 241% overpower in 30 seconds. The power decreasing rate for the short term is a little faster than the experimental data. The re-criticality power peak occurs at 3200 seconds with about 31% of the initial power, which is close to the experimental data of 27% power peak at 3420 seconds. But, this shows a higher deviation from the measured

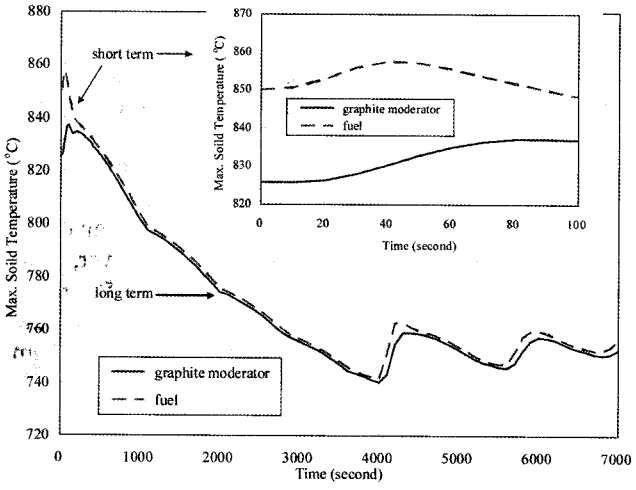

Fig. 12. Maximum Temperature Transient of the Fuel and Graphite Moderator after the 1mk-CRW ATWS

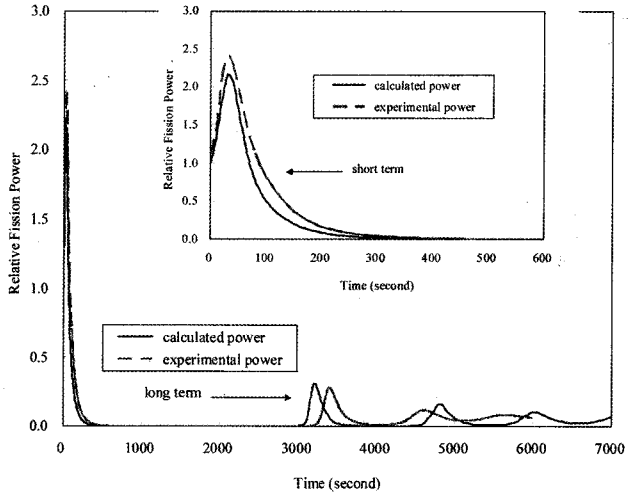

(a) Using the Rapid flow Coastdown Curve

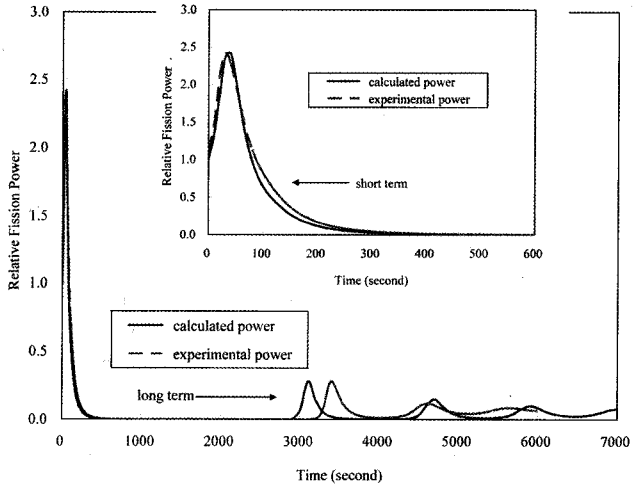

(b) Using the Slow Flow Coastdown Curve

Fig. 13. Reactor Power Transient after the 5mk-CRW ATWS

data of the reactor power transient in the short term than that of the 1mk-CRW ATWS. Based on the various calculations made by changing the flow coastdown curve or the point-kinetic parameters and models, it was found that the overpower level and the power decay curve in the short term were sensitive to the flow coastdown curve after the helium circulator trip. So, as shown in Fig. 13 (b), the change of the flow coastdown curve results in a reduction of the discrepancy between the predicted and the experimental data of the reactor power transient in the short term.

From investigating the net reactivity behavior after withdrawing the 5mk control rod, the occurrence times of peak net reactivity at 20 seconds and subcritical onset at 50 seconds are very similar to those of the 1mk reactivity insertion. The reactor core becomes critical again at 2100 seconds and reaches a re-critical peak reactivity at 3100 seconds. Compared to the small effects of the fuel, the reflector and the xenon concentration, the reactivities of the graphite moderator and the control rod mainly contribute to the net reactivity behavior. The fuel reactivity effect of the 5mk-CRW ATWS is obviously greater than that of the 1mk-CRW ATWS because the temperature gradient of the 5mk-CRW ATWS is higher than that of the 1mk-CRW ATWS. The minor effect of xenon is caused by the low initial xenon concentration of the HTR-10 reactor due to the low reactor power. This is consistent with the evaluation of the tests results [16], in which it was indicated that xenon caused the reactor to become critical again after 23.5 hours for the AVR [17], but the core temperature decrease caused the reactor to become critical again after only 0.7 hours at the HTR-10 because of the relatively small core volume.

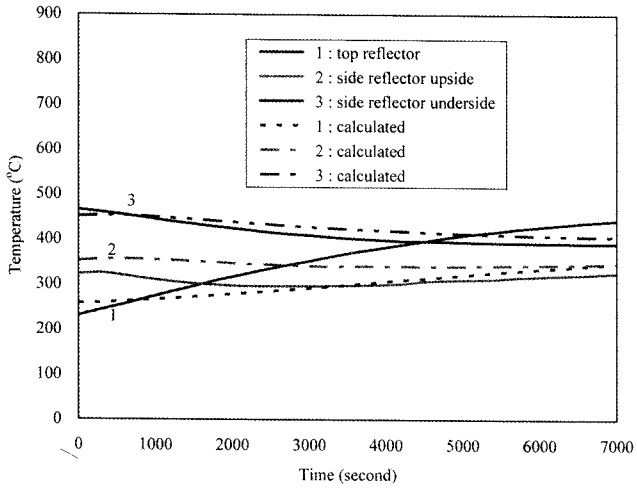

(a) Top and Side Reflectors

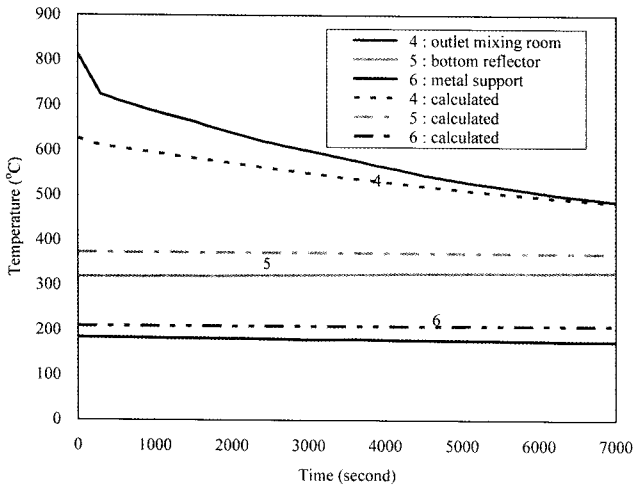

(b) Outlet Plenum, Bottom Reflector and Metal Support

Fig. 14. Solid Temperature Transient after the 5mk-CRW ATWS

Like the reactor power response behavior, due to a larger reactivity insertion, the fuel temperature increase of 28 °C in 60 seconds just after a CRW and the fuel temperature decrease rate of -2.03 °C/min after a subcritical onset (103 °C in 3100 seconds) are greater than those of the 1mk reactivity insertion. The moderator temperature reaches a peak increase of 30 °C at 220 seconds after the peak fuel temperature occurs.

Fig. 14 shows the behaviors of the solid temperatures in the reflectors and metal supports. The temperature of the top reflector is significantly increased, but the temperatures of the other parts are slowly decreased. The calculated temperature of the top reflector is increased by 91 °C in 7000 seconds, which is relatively small compared to the measured temperature increase of 212 °C. The temperatures of other reflectors and core structure parts are close to the measured data. The calculated temperature of the outlet mixing zone is under-predicted during 3000 seconds, and then converges to the measured data.

4. CONCLUSIONS

In this paper, the ATWS calculation results of the GAMMA+ code were compared with the HTR-10 experiments of a LOFC and two CRW ATWS tests by solving the point-kinetic equations simultaneously coupled with the thermal fluid heat transfer equations. The calculated results of the GAMMA+ code showed good agreement with the experimental power response behavior such as the power increasing and decreasing curve for the short term, and the re-criticality time and the power oscillation peak for the long term. It was found that the occurrence of the re-criticality in the HTR-10 after the ATWS is mainly caused by the graphite moderator reactivity feedback, but the effects of the fuel, the reflector, and xenon concentration are relatively small. The minor effect of xenon is caused by the low initial xenon concentration of the HTR-10 reactor due to the low reactor power. It is concluded that the GAMMA+ code is useful for an ATWS assessment to simulate a reactor power response by solving the point-kinetic equations for a VHTR design.

ACKNOWLEDGEMENTS

This work was supported by Nuclear Research & Development Program of the Korea Science and Engineering Foundation (KOSEF) grant funded by the Korean government (MEST). (grant code: M20701010003-08M0101-00310)

NOMENCLATURE

Δt	time step [sec.]
Δx, Δz	i-, j- direction grid size of (i,j) cell in core solid zone [m]
λ_{fuel}	thermal conductivity of fuel [W/m/ K]
λ_{eff}	effective thermal conductivity of core solid zone [W/m/ K]
φ	porosity of the fluid zone
φ_g	volume fraction of the graphite zone to a pebble sphere
$(\rho C_p)_{fuel}$	volumetric heat capacity in the fueled zone [J/m^3/ K]
$(\rho C_p)_w$	volumetric heat capacity in the unfueled zone [J/m^3/ K]
A_x, A_z	i-, j- direction cross-section area of (i,j) cell in core solid zone [m^2]
a_{gf}	specific surface area per volume [1/m]
h_g	heat conductance of the graphite [W/m^2/ K]
h_{gf}	defined as $h_g a_{gf}$ [W/m^3/ K]
$\dot{q}_N^{'''}$	volumetric heat production [W/m^3]
$\dot{q}_{gf}^{'''}$	volumetric heat transfer between the fueled zone and the graphite zone [W/m^3]
$\dot{q}_{sf}^{'''}$	volumetric heat transfer between the fluid zone and the solid part [W/m^3]
r	radial coordinate of the fueled zone [m]
T_{fuel}	1-D fuel temperature in the fueled zone [K]
T_o	fuel temperature at the outer mesh of the fueled zone [K]
T_i	fuel temperature at the i mesh of the fueled zone [K]
T_{wi}	multi-D core solid temperature at the surface of a fuel and graphite composite [K]
$T_{i,j}$	core solid temperature at (i,j) cell [K]
T_f	fluid temperature at the multi-D cell in core zone [K]
Vol_{ij}	volume of (i,j) cell in core solid zone [m^3]

ABBREVIATIONS

ATWS	anticipated transient without scram
CRW	control rod withdrawal
FPIC	full power initial core
LOFC	loss of forced cooling by a trip of the helium circulator
RCCS	reactor cavity cooling system
RPV	reactor pressure vessel
VHTR	very high temperature gas-cooled reactor
PBMR	pebble-bed modular reactor
PMR	prismatic modular reactor
1-D, 2-D, multi-D	one-dimensional, two-dimensional, multi-dimensional

REFERENCES

[1] Jonghwa Chang, et al, "A Study of a Nuclear Hydrogen Production Demonstration Plant", Nuclear Engineering and Technology, Vol. 39 No.2, 2007.4.

[2] Hong Sik Lim, Hee Cheon No, "GAMMA Multidimensional Multicomponent Mixture Analysis to Predict Air Ingress Phenomena in an HTGR", Nuclear Science and Engineering 152 (2006) 1-11, 2006.

[3] James J. Duderstadt, Louis J. Hamilton, "Nuclear Reactor Analysis", John Wiley & Sons, Inc, 1976.

[4] INET, "HTR-10 Experiments Report - Loss of Helium Flow without Reactor Scram", NH-JRC-P1-R06-009, KAERI/INET Internal Report, 2006.5.

[5] INET, "HTR-10 Experiments Report - Reactivity Insertion without Reactor Scram", NH-JRC-P1-R06-010, KAERI/INET Internal Report, 2006.5.

[6] Zongxin Wu, Dengcai Lini, Daxin Zhong, "The Design Features of the HTR-10", Nuclear Engineering and Design 218 (2002) 25-32, 2002.

[7] Ji Su Jun, HongSik Lim, Won-Jae Lee, "The Preliminary GAMMA Code Thermal Hydraulic Analysis of the HTR-10 Steady State Initial Core", 2006 KNS Spring Conference, 2006. 5.

[8] Ji Su Jun, Hong Sik Lim, Won-Jae Lee, "Final Report of IAEA CRP5 Benchmark Problem of HTR-10 Steady State Temperature Distribution (Rev. 1)", NHDD-KA06-RD011-01, KAERI Internal Report, 2006.11.

[9] Ji Su Jun, Hong Sik Lim, Won-Jae Lee, "The GAMMA Code Assessment of the HTR-10 Safety Demonstration Experiments - LOFC ATWS", 2007 KNS autumn conference, 2007.10.

[10] Ji Su Jun, Hong Sik Lim, Jae Man Noh, Won-Jae Lee, "The GAMMA Code Assessment of the HTR-10 Safety Demonstration Experiments - CRW ATWS", 2008 KNS spring conference, 2008.5.

[11] Hyun Chul Lee, Seung Wook Lee, Jae Man Noh, Won Jae Lee, "MARS-GCR/CAPP Coupled Multi-Physics Calculation for the OECD/NEA PBMR-400 Benchmark Problem", KNS Spring Meeting, Gyeongju, Korea, May 29-30, 2008.

[12] IAEA, "Benchmark Problems of the HTR-10 ; Prepared for the IAEA CRP-5 by INET", IAEA-TECDOC-xxx, on going version, 2005. 12.

[13] D.A. Nield, A. Bejan, "Convection in Porous Media", Springer-Verlag, New York, 1999.

[14] "Numerical Recipes: The Art of Scientific Computing", Cambridge University Press, 2007.

[15] J.P. Holaman, "Heat Transfer", McGraw-Hill, 1986.

[16] Shouyin Hu, Ruipian Wang, Zuying Gao, "Transient Tests on Blower Trip and Rod Removal at the HTR-10 ", Nuclear Engineering and Design 236 (2006) 677-680, 2006.

[17] Baumer R., et al, "AVR: Experimental High Temperature Reactor ; 21 Years of Successful Operation for a Future Energy Technology/Association of German Engineers (VDI)", The Society for Energy Technologies (Publ.), VDI-Verl, 1990.